Journal of Alloys and Compounds 595 (2014) 8–13

Contents lists available at ScienceDirect

Journal of Alloys and Compounds

journal homepage: www.elsevier.com/locate/jalcom

Effect of Sn loading on the photocatalytic aniline synthesis activity of TiO_2 nanospheres

R.M. Mohamed [a,b,c,*], E.S. Aazam [a]

[a] Chemistry Department, Faculty of Science, King Abdulaziz University, P.O. Box 80203, Jeddah 21589, Saudi Arabia
[b] Nanostructured Material Division Advanced Materials Department, Central Metallurgical R&D Institute, Helwan 11421, Cairo, Egypt
[c] Center of Excellence in Environmental Studies, King Abdulaziz University, P.O. Box 80216, Jeddah 21589, Saudi Arabia

ARTICLE INFO

Article history:
Received 15 December 2013
Received in revised form 14 January 2014
Accepted 21 January 2014
Available online 30 January 2014

Keywords:
TiO_2 nanospheres
Sn doping
Visible photocatalyst
Aniline

ABSTRACT

TiO_2 nanospheres and Sn/TiO_2 nanospheres were prepared by a hydrothermal method. The prepared samples were characterized by XRD, Pl, UV–Vis, BET, SEM, and TEM. The results reveal that Sn^{4+} replaces a small part of the Ti^{4+} from the TiO_2 lattice. Doping of Sn increases the surface area of the TiO_2 nanospheres. Doping of Sn leads to a decrease in the band gap of the TiO_2 nanospheres and increases the lifetime of the electron–hole recombination. Doping of Sn into the TiO_2 nanospheres enhances the photocatalytic activity of the TiO_2 nanospheres for the reduction of nitrobenzene to aniline under visible light. The optimal Sn loading was found to be 4 wt%. The photocatalytic activity of the 4 wt% Sn/TiO_2 nanospheres is approximately 80 times greater than the photocatalytic activity of the TiO_2 nanospheres.

1. Introduction

Nitrobenzene is reduced by hydrogenation to aniline, an important intermediate in the production of pigments, pesticides, dyes, and pharmaceuticals [1,2]. In the hydrogenation method, noble metals such as Pt, Pd, and Au and transition metals such as Cu and Ni are used as catalysts. The disadvantages of the hydrogenation process are that the hydrogenation method needs high temperatures and high hydrogen pressures [3,4]. Many researchers have studied the reduction of nitrobenzene to aniline using a photocatalyst at room temperature [5–7]. The previous studies of the reduction of nitrobenzene to aniline reported that the conversion and the selectivity were still low [8–10]. TiO_2 is by far the most popular photocatalyst used for the reduction of nitrobenzene to aniline because of the low price, lack of toxicity, high stability, and high photocatalytic activity [8–14]. The separation of ultrafine TiO_2 and a large band gap of 3.2 eV are the two serious problems that impede the commercial use of TiO_2. The development of the excitation of the photocatalyst by visible light must be studied. The semiconductor photocatalysts with a more negative conduction band have strong reductive activity. Nitrobenzene can be reduced to aniline by a photocatalyst with a conduction band potential lower than −0.486 V because $E_{C6H5NO2/C6H5NH2}$ = −0.486 V [15] vs. NHE. So the narrow band gap photocatalysts with a high negative value of the conduction band are effective for the photocatalytic reduction of nitrobenzene. TiO_2 has a wide band gap, which makes it useful in the ultraviolet region [16]. Scientists have tried to decrease the band gap of TiO_2 by many methods such as metal loading, doping, and sensitizing approaches [17–25]. In this work, we report a facile hydrothermal method to synthesize TiO_2 with Sn incorporated. To study the effect of Sn on the photocatalytic activity of TiO_2, the performance of prepared TiO_2 and Sn–TiO_2 nanosphere samples was studied for the photocatalytic reduction of nitrobenzene to aniline under irradiation by visible light.

2. Experimental

2.1. Synthesis of TiO_2 nanospheres

The hydrothermal method was used to prepare TiO_2 nanospheres. Titanium isobutoxide (3 mL) was added to a solution of 60 mL of anhydrous ethanol, 6 mL of nitric acid and 3 mL of deionized water with magnetic stirring for 60 min. HF (1.2 mL, 20%) was added to the above solution, and the resulting mixture was stirred for 60 min. The resulting mixture was transferred to an autoclave for 4 h at 180 °C. The precipitate was washed several times with ethanol. The resulting sample was dried under vacuum at 40 °C then calcined at 550 °C for 5 h.

* Corresponding author at: Chemistry Department, Faculty of Science, King Abdulaziz University, P.O. Box 80203, Jeddah 21589, Saudi Arabia. Tel.: +966 540715648; fax: +966 2 6952292.
E-mail address: redama123@yahoo.com (R.M. Mohamed).

http://dx.doi.org/10.1016/j.jallcom.2014.01.168
0925-8388/

Table 1
Chromatographic conditions applied for photocatalytic reduction of nitrobenzene.

	Reduction of nitrobenzene
Oven	50 °C for 5 min → 200 °C 50 → 200 °C at 10 °C/min
Detector	Type: FID Heater: 300 °C H_2 flow: 30 mL/min Air flow: 400 mL/min Makeup flow: 25 mL/min
Injection	Heater: 250 °C Pressure: 13.762 psi Total flow: 41.384 mL/min Septum purge flow: 3 mL/min Mode: split with ratio (10:1)
Column	(30 m × 0.32 μm × 0.25 μm)

2.2. Synthesis of Sn-doped TiO_2 nanospheres

In a typical synthesis of 3% Sn-doped TiO_2 photocatalyst, 3 mL of titanium isobutoxide was added to a solution of 60 mL of anhydrous ethanol, 6 mL of nitric acid, 45.75 mg of $SnCl_4{\cdot}5H_2O$, and 3 mL of deionized water under magnetic stirring for 60 min. HF (1.2 mL, 20%) was added to the above solution, and the resulting mixture was stirred for 60 min. The resulting mixture was transferred to an autoclave for 4 h at 180 °C. The precipitate was washed several times with ethanol. The resulting sample was dried under vacuum at 40 °C and then calcined at 550 °C for 5 h. Similarly, Sn-doped TiO_2 with molar ratios of 1%, 2%, 4%, and 5% was also synthesized with the other experimental conditions remaining unchanged.

2.3. Characterization techniques

X-ray diffraction (XRD) analysis was carried out at room temperature with a Bruker Axis D8 using Cu Kα radiation (λ = 1.540 Å). The specific surface area was calculated from N_2-adsorption measurements, which were obtained using a Nova 2000 series Chromatech apparatus at 77 K. Prior to the measurements, the samples were treated under vacuum at 120 °C for 2 h. The band gap of the samples was identified by UV–Visible diffuse reflectance spectroscopy (UV–Vis-DRS), which was performed in air at room temperature in the wavelength range of 200–800 nm using a UV/Vis/NIR spectrophotometer (V-570, JASCO, Japan). Transmission electron microscopy (TEM) was conducted with a JEOL-JEM-1230 microscope, and the samples were prepared by suspension in ethanol, followed by ultrasonication for 30 min. Subsequently, a small amount of this solution was placed onto a carbon-coated copper grid and dried before loading the sample into the TEM. X-ray photoelectron spectroscopy (XPS) studies were performed using a Thermo Scientific K-Alpha XPS, England. Photoluminescence (Pl) emission spectra were recorded with a Shimadzu RF-5301 fluorescence spectrophotometer. The surface morphology of the catalyst was examined using SEM JEOL 5410 (Japan).

2.4. Photocatalytic reduction of nitrobenzene

Photocatalytic reduction of nitrobenzene (NB) was carried out in a cylindrical Pyrex glass cell. The dimensions of the reactor are 200 mm in height and 28 mm in diameter. For each photocatalytic reaction, 50 mg of the photocatalyst was dispersed in 10 mL of NB in methanol solution by ultrasonication. To eliminate dissolved O_2 from the reaction mixture before illumination, pure nitrogen gas was passed through the photocatalytic reactor for 6 h. A 500 W Hg lamp with an optical UV cutoff filter was used for visible light illumination. The NB and the resulting photocatalytic products were analyzed by an Agilent GC 7890A model: G3440A Gas Chromatograph using a 19091 J-413 capillary column (30 m × 320 μm × 0.25 μm). The chromatographic conditions applied for photocatalytic reduction of nitrobenzene are summarized in Table 1.

3. Results and discussion

3.1. Characterization of the photocatalyst

3.1.1. XRD analysis

Fig. 1 shows the XRD patterns of the TiO_2 nanospheres and the Sn/TiO_2 nanospheres. The XRD patterns reveal that the TiO_2 anatase phase (JCPDS No. 21-1272) exists for all samples. We also noticed that Sn^{4+} ions replaced Ti^{4+} ions as shown in Fig. 1 as a shift of the peak plan (1 0 1) because the ionic radius and electronegativity of Ti^{4+} ions (68 pm) are close to the ionic radius and electronegativity of the Sn^{4+} ions (71 pm).

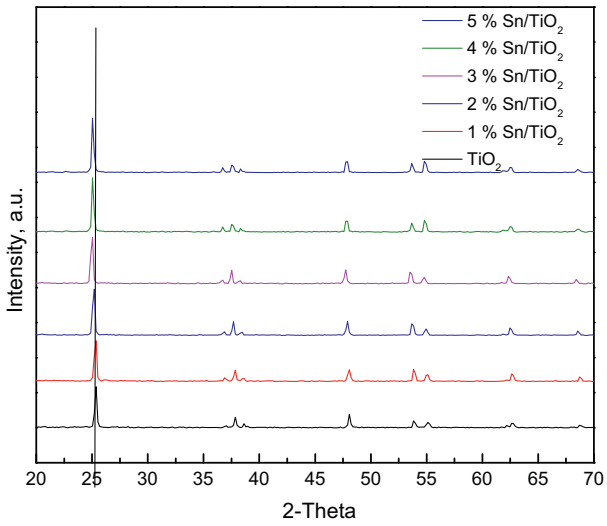

Fig. 1. XRD patterns of TiO_2 nanospheres and Sn/TiO_2 nanospheres.

3.1.2. SEM images

Fig. 2 shows the SEM images of the TiO_2 nanospheres (a); 1 wt% Sn/TiO_2 nanospheres (b); 2 wt% Sn/TiO_2 nanospheres (c); 3 wt% Sn/TiO_2 nanospheres (d); 4 wt% Sn/TiO_2 nanospheres (e); and 5 wt% Sn/TiO_2 nanospheres (f). The SEM images reveal that TiO_2 appears as uniform smooth nanospheres with 30–40 nm in diameter as shown in Fig. 1a. Fig. 1b–f reveal that the loading of Sn onto the TiO_2 makes its surface rough.

3.1.3. TEM images

Fig. 3 shows the TEM images of TiO_2 nanospheres (a) and 4 wt% Sn/TiO_2 nanosphere samples. The TEM images reveal that the shape of TiO_2 and Sn/TiO_2 is nanospherical. The surface of the TiO_2 nanospheres is smooth and uniform, but the surface of the Sn/TiO_2 nanospheres is rough.

3.1.4. XPS spectra

Fig. 4 shows the XPS spectra of the 4 wt% Sn/TiO_2 nanosphere sample. The XPS spectra (Fig. 4a–c) demonstrated that Sn, Ti, and O species were present, corresponding to binding energies of 486.6, 495, 458.7, 464.4, and 531.1 eV corresponding to the binding energies of Sn 3d, Ti 2p, and O 1s for Sn/TiO_2, respectively.

3.1.5. BET surface area measurement

Fig. 5 shows the adsorption–desorption isotherm of the TiO_2 and 4 wt% Sn/TiO_2 nanosphere samples. The BET measurements reveal that the type of isotherm for two samples is type IV, which indicates the presence of mesoporosity in the samples. Table 2 shows the BET surface of the TiO_2 and Sn/TiO_2 nanosphere samples. The BET measurements reveal that the BET surface areas of TiO_2, 1 wt% Sn/TiO_2, 2 wt% Sn/TiO_2, 3 wt% Sn/TiO_2, 4 wt% Sn/TiO_2, and 5 wt% Sn/TiO_2 samples are 70.0, 71.3, 71.9, 72.4, 72.8, and 72.5 m^2/g, respectively.

3.1.6. UV–Vis spectra

Fig. 6 shows the UV–Vis spectra of the TiO_2 and the Sn/TiO_2 nanosphere samples. The UV–Vis spectra reveal that the

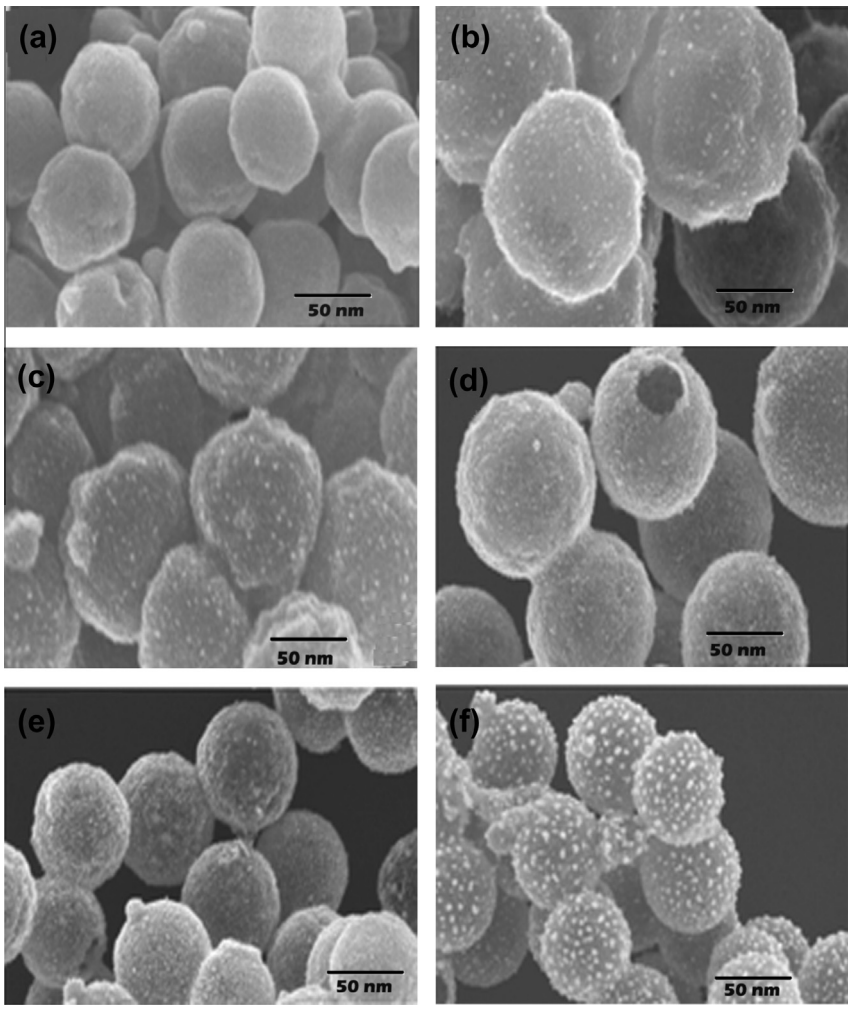

Fig. 2. SEM images of TiO_2 nanospheres (a); 1 wt% Sn/TiO_2 nanospheres (b); 2 wt% Sn/TiO_2 nanospheres (c); 3 wt% Sn/TiO_2 nanospheres (d); 4 wt% Sn/TiO_2 nanospheres (e); and 5 wt% Sn/TiO_2 nanospheres (f).

absorption edge of TiO_2 nanospheres is placed at 409 nm. Additionally, the UV–Vis spectra reveal that the loading of Sn leads to a shift in the absorption edge of 1 wt% Sn/TiO_2, 2 wt% Sn/TiO_2, 3 wt% Sn/TiO_2, 4 wt% Sn/TiO_2, and 5 wt% Sn/TiO_2 samples from 433, 443, 458, 469, and 480 nm, respectively. Therefore, loading of Sn leads to a red-shift to higher wavelengths. The calculated band gap from the UV–Vis spectra of TiO_2, 1 wt% Sn/TiO_2, 2 wt% Sn/TiO_2, 3 wt% Sn/TiO_2, 4 wt% Sn/TiO_2, and 5 wt% Sn/TiO_2 samples is 3.03, 2.87, 2.79, 2.70, 2.64, and 2.58 eV, respectively.

3.1.7. Pl spectra

Fig. 7 shows the Pl spectra of TiO_2 and Sn/TiO_2 nanospheres. The P1 spectra reveal that the Pl emission intensity decreased as the wt% of the Sn loading into the TiO_2 increased. Sn therefore acts as a photogenerated electron trap and increases the lifetime for recombination of electrons and holes. When the wt% of Sn increased from 1 to 4 wt%, the trapping of photogenerated electrons increased as shown in Fig. 7 as the decrease in Pl intensity. However, when the wt% of Sn increased above 4 wt%, some of the Sn covered the active sites of the TiO_2 and some of the Sn increased the recombination rate of electrons and holes [26–28].

3.2. Photocatalytic activity

3.2.1. Effect of the wt% of Sn on the photocatalytic activity of the TiO_2 nanospheres for production of aniline

Fig. 8 shows the effect of the wt% of Sn on the photocatalytic activity of TiO_2 nanospheres for production of aniline from nitrobenzene. The results reveal that the % of aniline production by TiO_2 nanospheres under visible light is very small (approximately 17%) because TiO_2 nanospheres absorb in the UV region and the experiment was carried out under visible light. Additionally, experimental results reveal that the increased wt% of Sn from 1 to 4 wt% increased the aniline production from 32% to 100% because Sn acts as a photogenerated electron trap and increases the lifetime for recombination of electrons and holes. However, the increased wt% of the Sn above 4 wt% decreases the aniline production to 96% because some of the Sn covered the active sites of TiO_2 and some of the Sn increased the recombination rate of the electron and hole [26–28] and hence photocatalytic activity decreased. The optimal wt% of Sn is 4 wt% where the level of aniline production is 100% after 90 min reaction time.

3.2.2. Photochemical stability

For practical application of a photocatalyst, two factors related to recycling should be considered: the ease of separation from

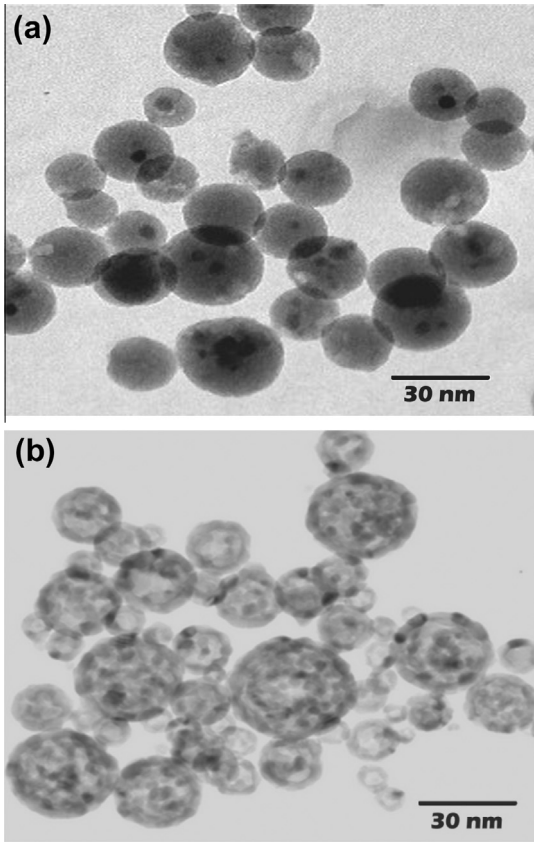

Fig. 3. TEM images of TiO_2 nanospheres (a) and 4 wt% Sn/TiO_2 nanospheres.

the solution and the stability against inactivity and photocorrosion after long-term usage. We therefore reused the 4 wt% Sn/TiO_2 nanospheres five times to test stability. After five catalysis cycles for reduction of nitrobenzene, the 4 wt% Sn/TiO_2 nanospheres do not show dramatic deactivation (Fig. 9) and are nearly unchanged in crystal phase, composition, and absorption. This result indicates high photostability and recyclability of the catalyst.

3.2.3. Mechanisms

Gas chromatographic (GC) results showed that the main products were nitrosobenzene and aniline. The mechanism of the photocatalytic reduction of NB over the 4 wt% Sn/TiO_2 nanosphere sample follows: (1) Production of photogenerated hole–electron pairs. When irradiated by photoelectrons with energy equal to or larger than its band gap, electrons transfer from the valence band to the conduction band, thus producing oxidative photogenerated valence holes (h^+) and reductive conduction electrons (e−) (Eq. (1)). (2) Photogenerated holes and electrons without recombination move to the photocatalyst surface. (3) Chemical reactions between photogenerated carriers and adsorbents. The holes are captured by a CH_3OH solvent, producing HCHO oxide and reductive $H^{\cdot}$ (Eqs. (2) and (3)). NB is reduced by photogenerated electrons and H, thereby producing nitrosobenzene and aniline (Eq. (4)).

$$Sn/TiO_2 \xrightarrow{\text{Visible light}} Sn/TiO_2(e^- + h^+) \quad (1)$$

$$CH_3OH + h^+ \rightarrow CH_3O^{\cdot} + {}^{\cdot}CH_2OH \quad (2)$$

$$CH_3O^{\cdot} + {}^{\cdot}CH_2OH + \rightarrow 2H^{\cdot} + 2HCHO \quad (3)$$

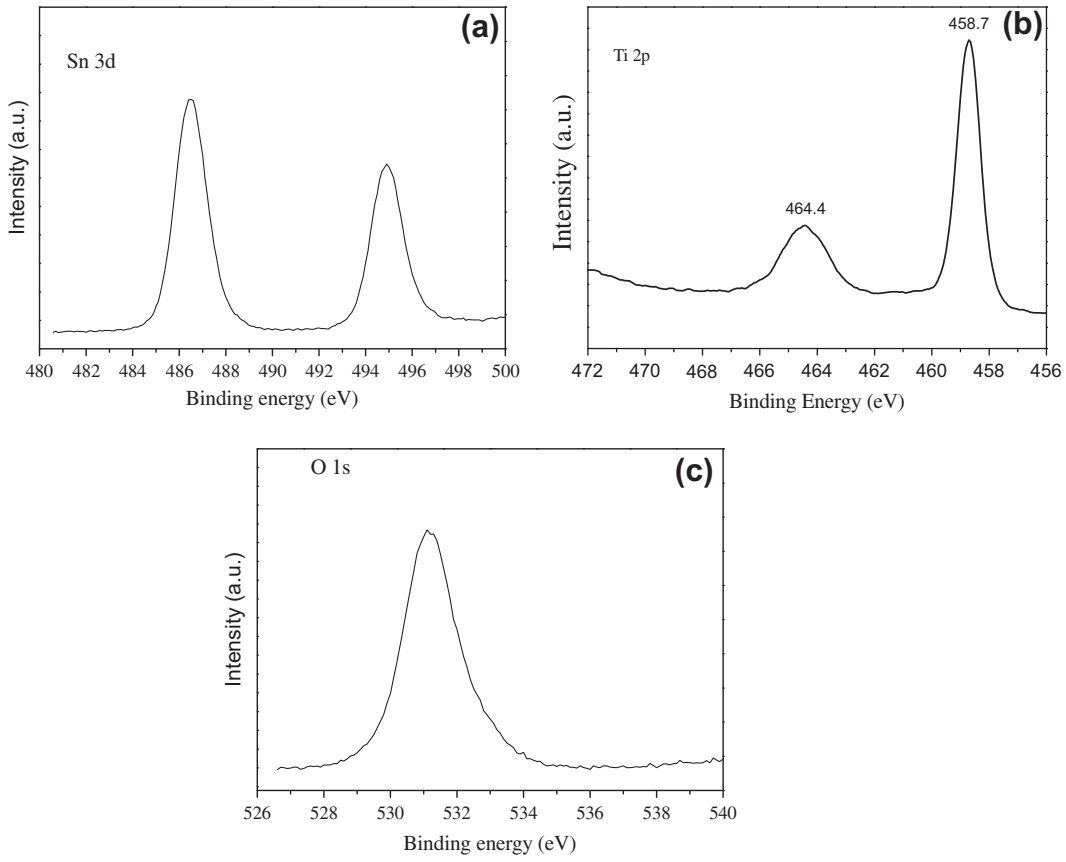

Fig. 4. XPS spectra for 4 wt% Sn/TiO_2 nanospheres, (a) for Sn 3d; (b) for Ti2p; and (c) for O1S.

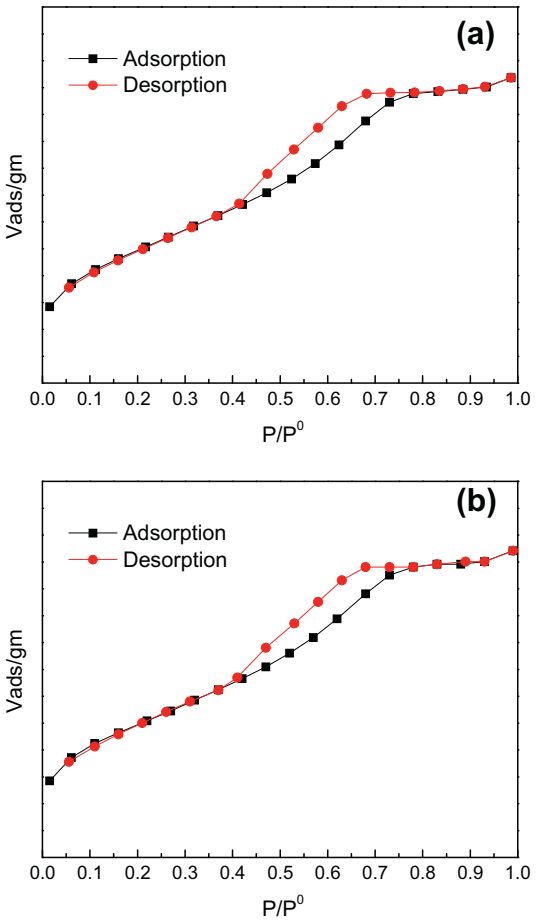

Fig. 5. N_2 adsorption–desorption isotherm of (a) TiO_2 and (b) 4 wt% Sn/TiO_2 nanospheres.

Table 2
The surface area of TiO_2 and Sn/TiO_2 samples.

Sample	BET (m^2/g)
TiO_2	70.0
1% Sn/TiO_2	71.3
2% Sn/TiO_2	71.9
3% Sn/TiO_2	72.4
4% Sn/TiO_2	72.8
5% Sn/TiO_2	72.5

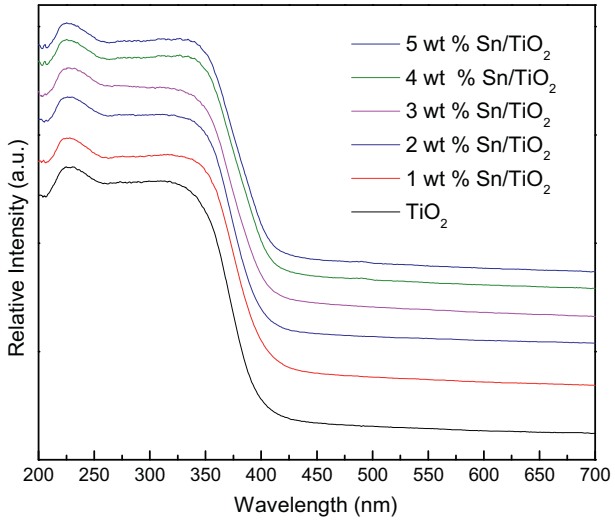

Fig. 6. UV–Vis spectra of TiO_2 and Sn/TiO_2 nanospheres.

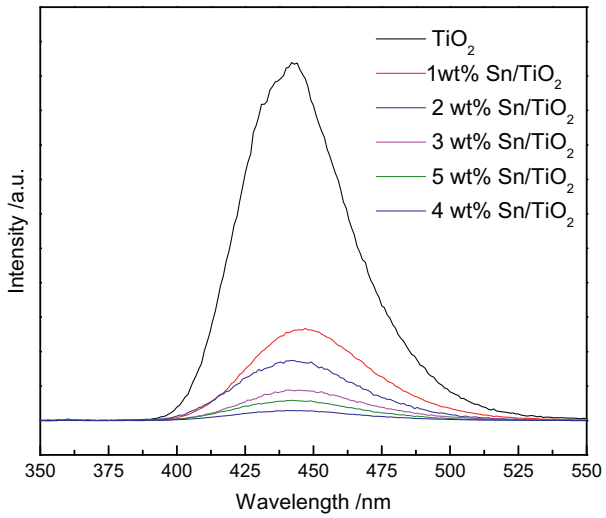

Fig. 7. Pl spectra of TiO_2 and Sn/TiO_2 nanospheres.

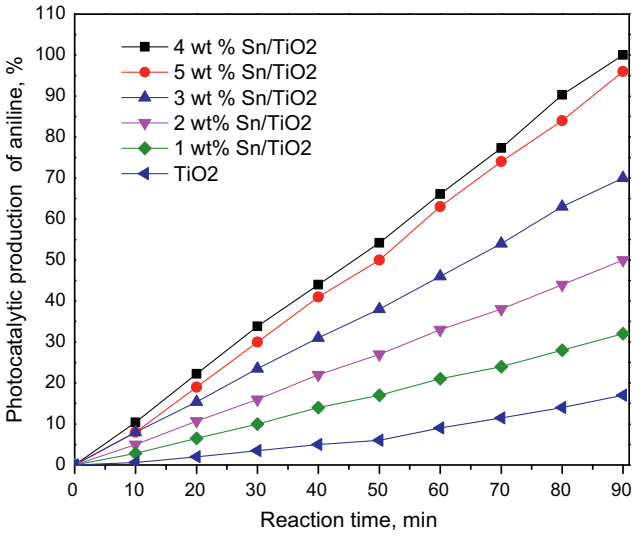

Fig. 8. Effect of the wt% of Sn on photocatalytic production of aniline.

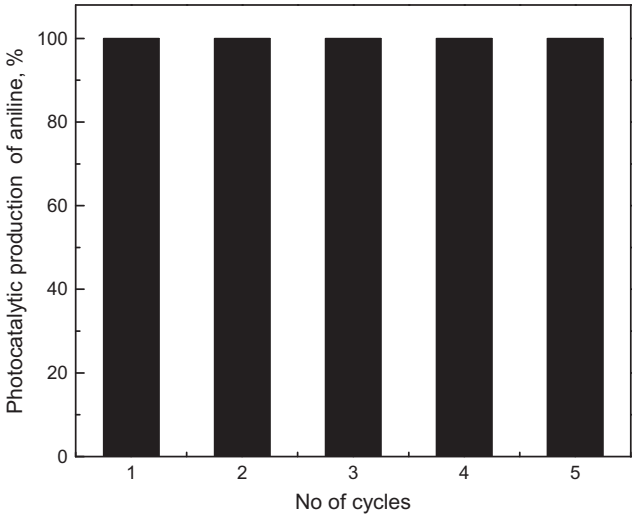

Fig. 9. Reuse of photocatalysts in the photocatalytic production of aniline.

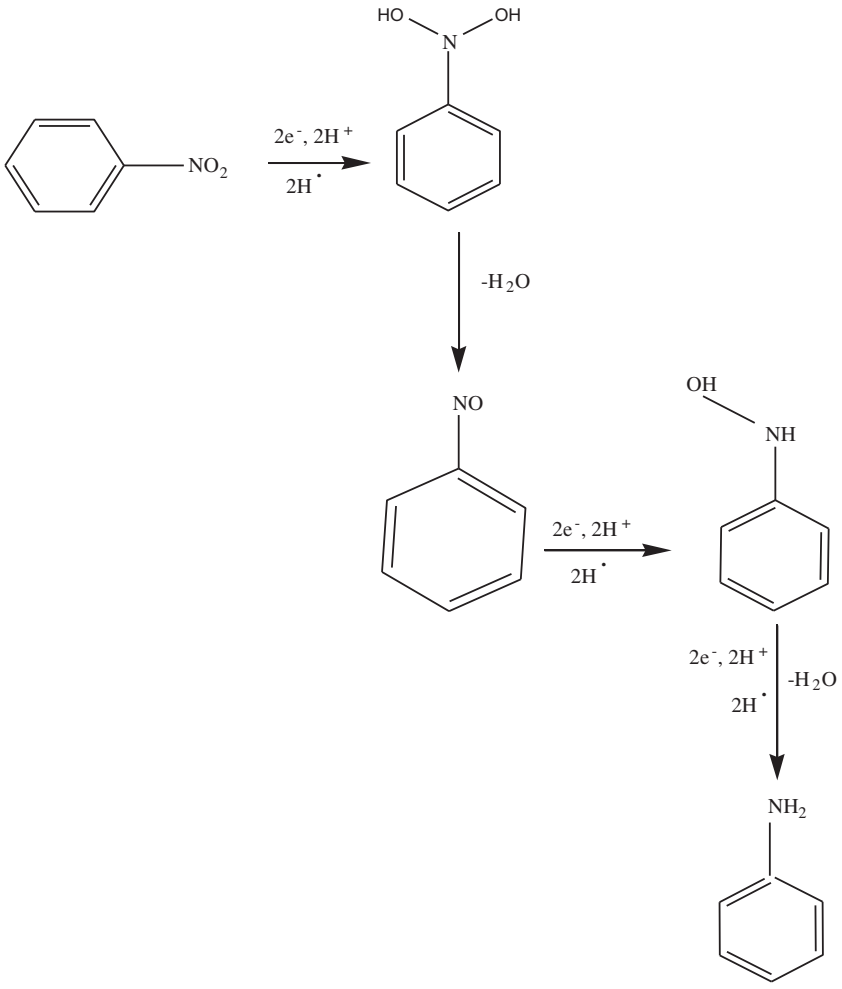

(4)

4. Conclusions

In summary, TiO_2 and Sn/TiO_2 nanosphere nanophotocatalysts were prepared using the hydrothermal method. The photocatalytic results for production of aniline from reduction of nitrobenzene under visible light show that Sn/TiO_2 nanospheres have a high photocatalytic activity with respect to TiO_2 nanospheres. The wt% of Sn plays an important role in the photocatalytic production of aniline. We found that 4 wt% of Sn/TiO_2 is the optimal wt% of Sn at which 100% aniline production was achieved after a 90-min reaction time. The 4 wt% Sn/TiO_2 nanospheres can be used five times without loss of photocatalytic activity.

References

[1] A. Corma, P. Concepcion, P. Serna, Angew. Chem. Int. Ed. 46 (2007) 7266–7269.
[2] J. Wang, Z. Yuan, R. Nie, Z. Hou, X. Zheng, Ind. Eng. Chem. Res. 49 (2010) 4664–4669.
[3] S.-P. Lee, Y.-W. Chen, J. Mol. Catal. A: Chem. 152 (2000) 213–223.
[4] H. Li, Q. Zhao, Y. Wan, W. Dai, M. Qiao, J. Catal. 244 (2006) 251–254.
[5] S.O. Flores, O. Rios-Bernij, M.A. Valenzuela, I. Córdova, R. Gómez, R. Gutiérrez, Top. Catal. 44 (2007) 507–511.
[6] S. Fuldner, P. Pohla, H. Bartling, S. Dankesreiter, R. Stadler, M. Gruber, A. Pfitzner, B. Konig, Green Chem. 13 (2011) 640–643.
[7] J.L. Ferry, W.H. Glaze, Langmuir 14 (1998) 3551–3555.
[8] S. Chen, H. Zhang, X. Yu, W. Liu, Chin. J. Chem. 28 (2010) 21–26.
[9] F. Mahdavi, T.C. Bruton, Y. Li, J. Org. Chem. 58 (1993) 744–746.
[10] J.L. Ferry, W.H. Glaze, J. Phys. Chem. B 102 (1998) 2239–2244.
[11] G. Liu, X. Li, J. Zhao, S. Horikoshi, H. Hidaka, J. Mol. Catal. A: Chem. 153 (2000) 221–229.
[12] H.-P. Dai, K.-K. Shiu, Electrochim. Acta 43 (1998) 2709–2715.
[13] S.D. Rychnovsky, R. Vaidyanathan, T. Beauchamp, R. Lin, P.J. Farmer, J. Org. Chem. 64 (1999) 6745–6749.
[14] M. Zhang, C. Chen, W. Ma, J. Zhao, Angew. Chem. Int. Ed. 120 (2008) 9876–9879.
[15] S. Balasubramanian, J. Lumin. 106 (2004) 69–76.
[16] M.Y. Abdelaal, R.M. Mohamed, J. Alloys Comp. 576 (2013) 201–207.
[17] R.M. Mohamed, E.S. Aazam, Chin. J. Catal. 33 (2) (2012) 247–253.
[18] R.M. Mohamed, Desalination Water Treat. 50 (2012) 147–156.
[19] R.M. Mohamed, D.L. McKinney, W.M. Sigmund, Mater. Sci. Eng. R 73 (2012) 1–13.
[20] R. M. Mohamed, Elham S. Aazam, Journal of Nanotechnology, vol. 2012, Article ID 794874, pp. 9.
[21] R.M. Mohamed, Elham S. Aazam, J. Alloys Comp. 509 (2011) 10132–10138.
[22] R.M. Mohamed, I.A. Mkhalid, J. Alloys Comp. 501 (2010) 301–306.
[23] R.M. Mohamed, I.A. Mkhalid, J. Alloys Comp. 501 (2010) 143–147.
[24] R.M. Mohamed, E.S. Baeissa, J. Alloys Comp. 558 (2013) 68–72.
[25] R.M. Mohamed, E.S. Baeissa, Appl. Catal. A 464–465 (2013) 218–224.
[26] Y. Ikuma, H. Bessho, Int. J. Hydrogen Energy 32 (2007) 2689–2692.
[27] Y.X. Li, G.X. Lu, S.B. Li, Appl. Catal. A 214 (2001) 179–185.
[28] X.L. Fu, J.L. Long, X.X. Wang, D.Y.C. Leung, Z.X. Ding, L. Wu, Z.Z. Zhang, Z.H. Li, X.Z. Fu, Int. J. Hydrogen Energy 33 (2008) 6484–6491.